

# Transparent polycrystalline alumina using spark plasma sintering: Effect of Mg, Y and La doping

Michael Stuer<sup>a,b</sup>, Zhe Zhao<sup>b,\*</sup>, Ulrich Aschauer<sup>a</sup>, Paul Bowen<sup>a</sup>

<sup>a</sup> Powder Technology Laboratory, Material Science Institute, Swiss Federal Institute of Technology, CH-1015, Lausanne, Switzerland

<sup>b</sup> Department of Physical, Inorganic and Structural Chemistry, Arrhenius Laboratory, Stockholm University, SE-10691, Stockholm, Sweden

Received 7 July 2009; received in revised form 13 November 2009; accepted 1 December 2009

Available online 22 December 2009

## Abstract

Transparent polycrystalline alumina (PCA) is a promising replacement for sapphire. Its optical properties however are highly dependent on the grain size and residual porosity which need to be controlled for real inline transmittances (RIT), that are high enough for possible applications.

To achieve high RITs, doping as well as pressure assisted sintering is often used. In this study spark plasma sintering (SPS) and doping are investigated. A systematic experimental design is used to study the influence of Mg, Y and La single or co-doping (75–450 ppm) as well as the SPS sintering pressure and temperature on the RIT and grain size of PCA.

Using optimized sintering parameters, RITs of >50% were attained in the visible wavelength (640 nm) for 0.8 mm thick samples for almost all doping strategies. The best RIT of 57% was for triple-doped samples at a total dopant level of 450 ppm. These results are significantly better than previously published SPS studies and illustrate that SPS sintered alumina can attain high and reproducible optical transmittances under various doping and sintering conditions.

© 2009 Elsevier Ltd. All rights reserved.

**Keywords:** Al<sub>2</sub>O<sub>3</sub>; Sintering; Optical properties; SPS

## 1. Introduction

Over recent years, attempts have been made to replace sapphire by transparent polycrystalline alumina (PCA)<sup>1–6</sup> for both economic and ecological reasons.

The most important parameters controlling the degree of transparency achievable for polycrystalline materials are the grain size (e.g. light scattering by grains  $\gamma_G$ )<sup>1</sup> and the porosity (e.g. light scattering by pores  $\gamma_P$ )<sup>7</sup> as can be seen from the model for the real inline transmittance (RIT) given by Eqs. (1)<sup>8</sup> and (2):

$$\text{RIT} = \frac{I}{I_0} = (1 - R_S) \exp(-\gamma_{\text{tot}} D) \quad (1)$$

$$\gamma_{\text{tot}} = \gamma_G + \gamma_P + \dots = \frac{3\pi^2 r \Delta n^2}{\lambda_0^2} + \frac{3V_P Q_{\text{eff}}}{4r_m \exp(3.5\delta^2)} + \dots \quad (2)$$

with  $I_0$  and  $I$  the light beam intensities before and after travelling through a PCA sample with an apparent thickness  $D$ ;  $R_S$  the total normal surface reflectance ( $R_S(\text{Al}_2\text{O}_3) = 0.14$ ) and  $\gamma_{\text{tot}}$  the total scattering (absorption) coefficient;  $\gamma_G$  and  $\gamma_P$  the scattering contributions from the grains and the pores, respectively;  $r$  the (average) grain radius;  $\Delta n$  the (average) refractive index change between two adjacent grains ( $\Delta n_{\text{max}} = n_o - n_e = 0.008$ );  $\lambda_0$  the wavelength of the incident light in vacuum;  $V_P$  the specific pore volume;  $r_m$  the radius of the mode of the pore size distribution;  $\delta$  the standard deviation factor for a lognormal distribution and  $Q_{\text{eff}}$  an effective dimensionless scattering efficiency of the pores. The simulated contributions of grains and pores on the RIT are illustrated in Fig. 1 and described more in detail elsewhere.<sup>1,7</sup> This light scattering theory predicts the requirement of an average grain size diameter below 250 nm and a density above 99.995 vol.% for PCA to be competitive with sapphire in terms of RIT in the visible range (PCA > 80%; sapphire = 86%).

Over the last decade, several groups have tried to produce high-RIT PCA samples with two different strategies, namely natural sintering coupled with post-hot isostatic pressing (HIP) and spark plasma sintering (SPS).

\* Corresponding author.

E-mail address: [zhao@inorg.su.se](mailto:zhao@inorg.su.se) (Z. Zhao).

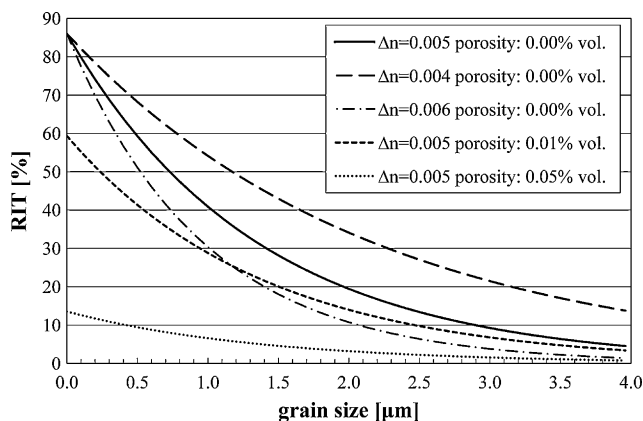


Fig. 1. Influence of grain size diameter, porosity (pore diameter 20 nm) and average refractive index change according to the optical model (Eq. (1)) on the RIT of PCA.

For post- HIP treated samples, results for undoped,<sup>5</sup> single-doped ( $\text{Mg}^{2+}$ ,  $\text{Ti}^{4+}$ )<sup>1,3,9</sup> and co-doped ( $\text{Ca}^{2+}$ - $\text{Ti}^{4+}$ )<sup>10</sup> PCA have been reported so far. This method gave fairly reproducible RITs between different groups with values up to 65%. However only Krell et al. reached RITs as high as 72%.<sup>5</sup> From some of these studies, it appeared that achieving “full” density without extensive grain growth can be favored by defect free green body processing.<sup>5,11</sup> Defect free high density green body fabrication gives a more homogeneous porosity distribution. This allows the pores to close as late as possible during the sintering cycle, reduces the sintering temperature<sup>5,11</sup> and retards the occurrence of grain growth.<sup>12,13</sup> As well as processing, the quality of the starting powder also plays a key role. Due to the very limited solubility of ions in  $\text{Al}_2\text{O}_3$  (in the ppm range), the grain boundary composition can be affected by segregated dopants or impurities, the powder should thus be of very high purity. Selective doping can further enhance densification versus grain growth by promoting densification and reducing the grain boundary mobility.<sup>9,14,15</sup>

For spark plasma sintered PCA samples, reported results<sup>2,16</sup> have been less promising, with a maximum RIT of 35% ( $\lambda = 640$  nm, thickness 1 mm; calculated RIT of 40% for 0.8 mm thickness according to Eq. (3)).<sup>16</sup> Reproducibility between different groups seems to be an issue and the achieved RITs are not in the range of those obtained with traditional sintering methods. However, careful powder processing to avoid agglomeration or contamination as well as improvements of the SPS sintering parameters should help to show the benefits of SPS.<sup>17</sup> Furthermore, in all the SPS studies reported to date the graphite dies have been loaded directly with the alumina powder (i.e. no green body).

No systematic research has been reported concerning the fabrication of doped polycrystalline alumina by SPS. In this study the effects of Mg, Y and La doping (single and combined) on the microstructure and light transmittance (i.e. RIT) of spark plasma sintered PCA were systematically evaluated.

Magnesium has been chosen due to its effects on grain boundary/surface diffusion<sup>14,18</sup> and grain boundary mobility,<sup>14,18</sup> the reported surface roughening<sup>19,20</sup> and its liquid scavenger<sup>19,21</sup>

effects. It is expected to enhance densification (e.g. by lowering the activation energy), avoid abnormal or anisotropic grain growth as well as influence the atomic arrangement and thus potentially the dopant cation solubility in the grain boundary area (e.g. oxygen vacancies).

Yttria has mainly been reported to increase creep resistance of alumina and to hinder grain growth during sintering.<sup>22,23</sup> It has a very low solubility in alumina and thus strongly segregates at grain boundaries<sup>24–26</sup> where it hinders diffusion processes and causes solute drag to occur. Its effects on the diffusion processes might be linked to the recently reported pattern formation of Y atoms at specific grain boundaries.<sup>25</sup>

The larger cation size of lanthanum compared to yttria but identical valence leads us to expect La to have stronger effects than yttria. Although both inhibit densification and grain growth, La has been reported to be the better grain growth inhibitor whereas Y is the better densification inhibitor<sup>15</sup> (c.f. pattern formation<sup>25</sup>).

The solubility of the selected dopants is very limited in alumina. The solid solution limits above which segregation or segregation plus precipitation occurs are commonly admitted to be in cationic ratios ( $[\text{dopant}]/[\text{Al}]$ ) in the ppm range (for  $\text{Mg} < 200$  ppm<sup>27</sup> and for Y and La even lower).

Although the effects of these dopants have been extensively reported in the literature, their effect may be different due to changes in kinetics when using SPS, where sintering of pieces takes several minutes rather than hours for natural sintering. The aim of this work is to provide a basic approach to achieve reproducible high-RIT ceramics by SPS and to better evaluate its application for the production of transparent PCA.

## 2. Materials and experimental method

The powder used was a polyhedral near-spherical high purity  $\alpha$ - $\text{Al}_2\text{O}_3$  with a median particle size  $D_{v50}$  of 510 nm, a total impurity concentration of less than 0.01 mass% ( $\leq 5$  ppm for Si, Na, Mg, Cu and Fe) and a specific surface  $S_{\text{BET}}$  of 4.2  $\text{m}^2/\text{g}$ .

Doping was carried out by dispersing 25 g of the powder in 60 mL 0.01 M  $\text{HNO}_3$  and adding the required dopant solutions  $\text{Mg}(\text{NO}_3)_2 \cdot 6\text{H}_2\text{O}$ ,  $\text{Y}(\text{NO}_3)_3 \cdot 6\text{H}_2\text{O}$ ,  $\text{La}(\text{NO}_3)_3 \cdot 6\text{H}_2\text{O}$  (purity  $>99\%$ , dissolved in 0.01 M  $\text{HNO}_3$ ) to achieve the desired cationic dopant ratio. After the dopant addition, 0.01 M  $\text{HNO}_3$  was added to reach a final volume of 80 mL. The suspension was stirred for 5 min and then treated for 10 min in an ultrasonic bath. The suspension was then frozen in liquid nitrogen and freeze-dried during approximately 45 h ( $-50$  °C @ 0.08–0.1 mbar, Alpha 1-4, Christ, Germany).

All single, double and triple dopant combinations of the 3 dopants Mg, Y and La were prepared for a total cationic dopant ratio of 225 ppm and 450 ppm resulting in 14 different doped powders. These different powders are referred to as 225:M00, 450:MYL, etc. to indicate the total cationic dopant ratio as well as the dopant elements (M = magnesium, Y = yttrium, L = lanthanum; all dopants were added in equal fractions of the total cationic ratio for double and triple doping). No calcination was performed before sintering. As a reference

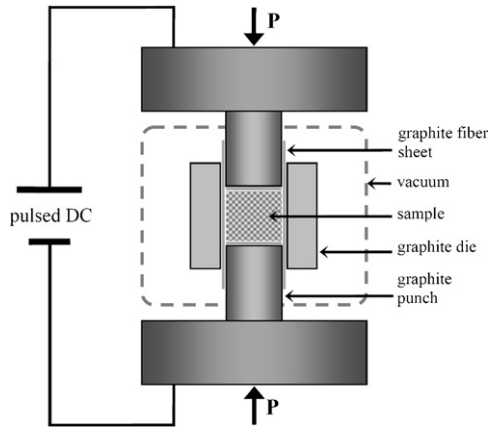


Fig. 2. Simplified illustration of an SPS installation.

baseline, the as-received and freeze-dried pure alumina powders have also been investigated.

For SPS sintering (Dr. Sinter 2050, Sumitomo Coal Mining Co., Tokyo, Japan) 0.8 g of powder was loaded into a graphite dye (Ø 12 mm), the internal surface of which was covered with a graphite fiber sheet to avoid direct contact between the powder compact and the graphite die (Fig. 2). The sintering temperature was measured by an optical pyrometer focused on a small cavity in the graphite die (distance between powder and cavity bottom was 5 mm). For maximum reproducibility, the sintering temperature and pressure were controlled by automatic controller units.

For all 16 different powders (doped and undoped), the influence of the sintering pressure and the sintering temperature were investigated according to an experimental matrix (Fig. 3). The RIT and grain size results were analyzed by statistical analysis of variance (factorial ANOVA)<sup>28</sup>: instead of conducting different series of independent experiments, they can be combined into one matrix, allowing the effect of interacting parameters to be examined as well as giving the statistical significance of variations of properties as a function of the different experimental parameters. The effect of the parameters, doping, temperature,

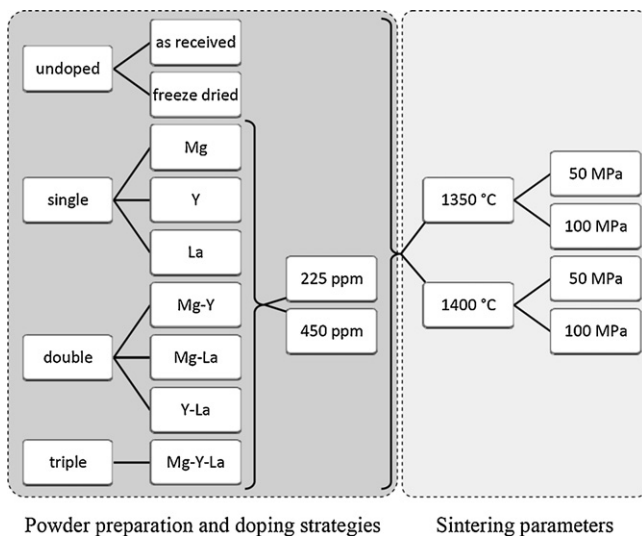


Fig. 3. Illustration of the studied experimental plan.

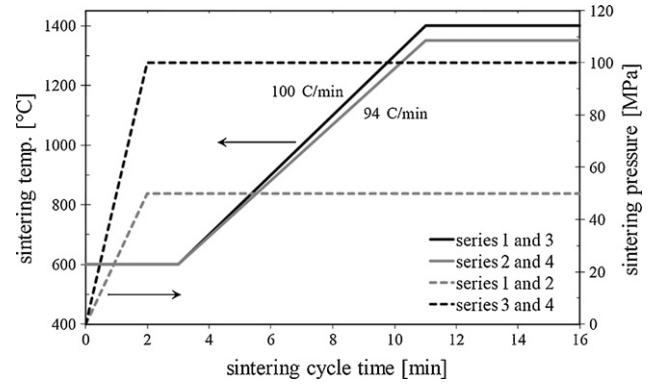


Fig. 4. Temperature and pressure cycles during SPS sintering.

pressure and possible interactions between them on the measured property (i.e. RIT or grain size) are determined within a confidence interval of 95% ( $p \leq 0.05$ ) according to standard statistical analysis.<sup>28</sup> The final sintering temperature was reached in 8 min after a dwell for 3 min at 600 °C. The uniaxial pressure was raised to the final sintering pressure during the first 2 min of the dwell at 600 °C. The exact cycles for each series are summarized in Fig. 4. The pulse sequence for the SPS applied voltage for all the samples was 12:2 (i.e. 12 on/2 off).

After sintering, the samples were polished down to a thickness of 1 mm to get parallel surfaces with a mirror-like quality using diamond pastes. The transmittance measurements were made with a UV–VIS spectrometer (UV-VIS-NIR Lambda 900, PerkinElmer, USA) in the wavelength range from 300 nm to 1000 nm. To assure that only the real-in line transmitted (RIT) light was measured, two metallic shields each with a hole of 4 mm diameter were inserted in the light path (Fig. 5). By this method no light scattered by more than 1.2° will reach the detector. As this is the maximum angle (border to border), this method can be assumed to be comparable to the laser RIT measurement (<0.5°) described by Krell et al.<sup>3</sup> Note that without shields, the inline transmittance measurement would include more scattered light and therefore the RIT would appear higher.

The RIT values given in this paper are the values at 640 nm for 0.8 mm thick samples to compare with other published RIT results. These values have been calculated from the measured 1 mm thick samples according to Eq. (3)<sup>3</sup>:

$$RIT(t_2) = (1 - R_S) \left( \frac{RIT(t_1)}{1 - R_S} \right)^{t_2/t_1} \quad (3)$$

where  $RIT(t_i)$  ( $i = 1, 2$ ) is the RIT for a sample thickness  $t_i$ .

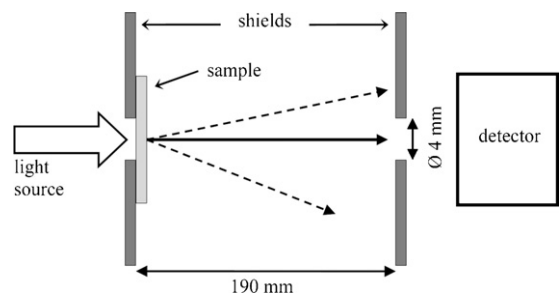


Fig. 5. Transmittance measurement setup.

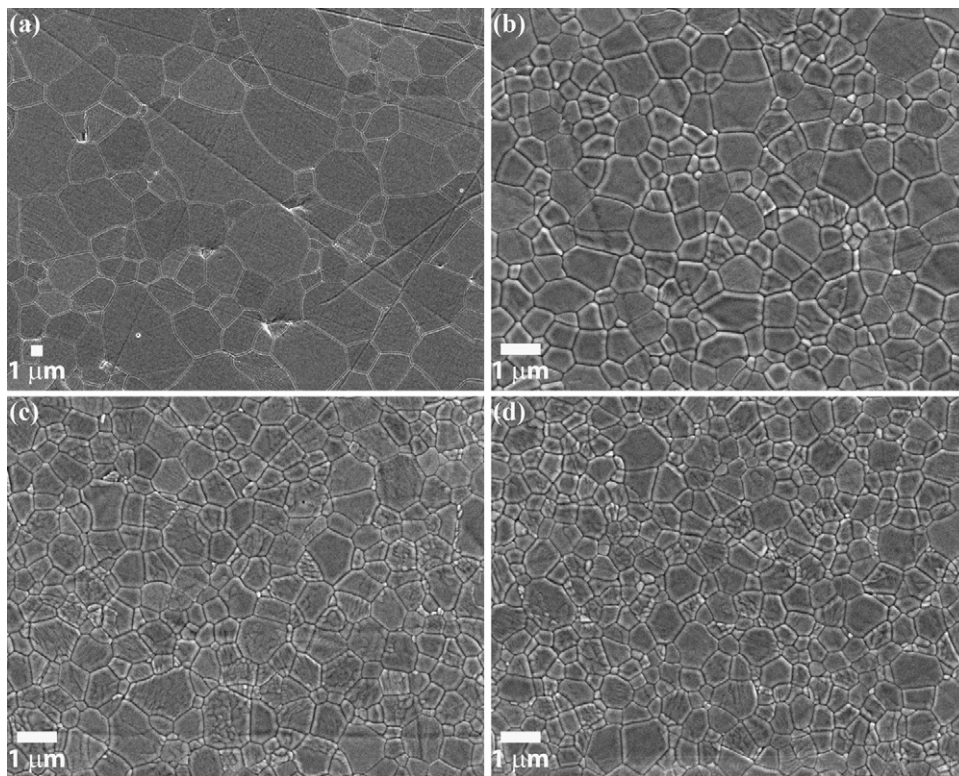


Fig. 6. Microstructures after thermal etching at 1350 °C (@ 100 MPa) sintered samples. (a) Pure (b) 225:M00, (c) 225:0Y0, and (d) 225:00L.

SEM pictures (FEG JSM-7000, JEOL, Japan) for grain size determination have been taken after thermal etching in air at 1150 °C for 30 min (heating rate 10 °C/min). The average line intercept method has been used, applying a correction factor of 1.56.<sup>29</sup>

### 3. Results and discussion

#### 3.1. General discussion

First of all it is important to note that the grain shapes obtained with different doping strategies (Fig. 6(b)–(d)) could all be treated as being isotropic and the grains can therefore be approximated by spheres in the light scattering model. Due to the isotropic nature of the microstructure, the observed RIT changes can mainly be attributed to grain size and density changes resulting from changes in doping and sintering parameters.

As illustrated in Fig. 1, the RIT is very sensitive to the residual porosity, the grain size and the average refractive index change ( $\Delta n$ ) between adjacent grains. In general, increasing the grain size reduces the RIT (samples become translucent) and increasing the porosity leads to opacification (samples become white or milky).

To take into account the birefringence of alumina, Apetz and van Bruggen proposed the  $\Delta n$  change to be close to 0.005.<sup>1</sup> Assuming no residual porosity (e.g. excluding milky samples) and applying the least mean square method to evaluate the best fit to our experimental results of RIT versus grain size, the  $\Delta n$  was determined to be 0.0053. The  $\Delta n$  evaluation is further being investigated by the electron backscatter diffraction (EBSD) tech-

nique, where knowledge of the grain orientations will allow us to calculate an average  $\Delta n$ . Archimedes density measurements could not reveal any significant density changes and all the samples are more than 99.95% dense. To evaluate the densities between the samples qualitatively, the experimental RITs as a function of the grain sizes are plotted in Fig. 7, as well as some selected theoretical curves.

All the samples, except the samples from the series sintered at 1350 °C and 50 MPa (points circled Fig. 7), can be assumed to be equally dense >99.99% with reasonable accuracy, as all the experimental points are close to the 0–0.01 vol.% optical model predictions. This facilitates the discussion of the doping effects given in the following sections.

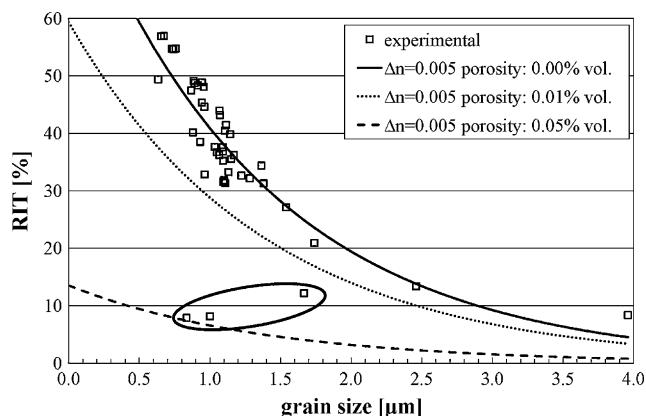


Fig. 7. RIT as a function of grain size diameter and model curves (Eq. (1)) with varying residual porosities (pore diameter 20 nm).

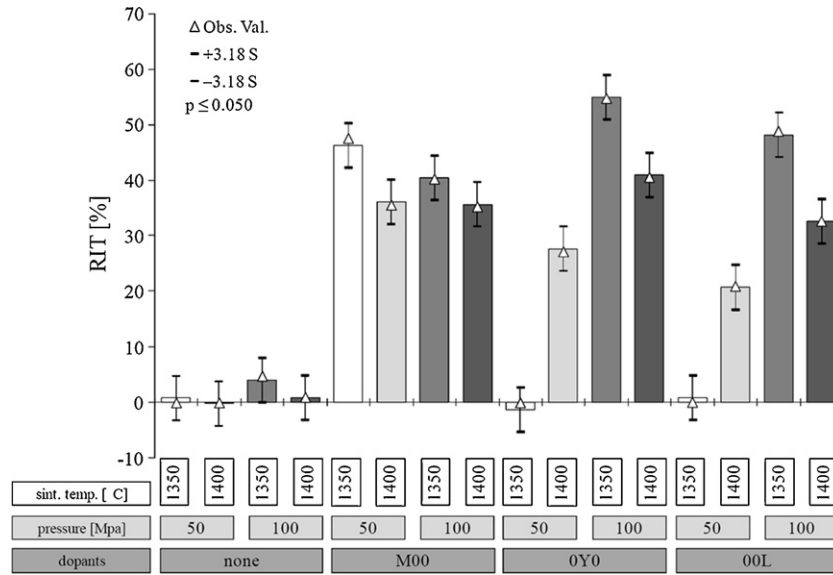


Fig. 8. Real inline transmittance as a function of dopant elements (450 ppm), sintering pressure and final sintering temperature. Heating rate:  $\sim 100^\circ\text{C}/\text{min}$ . Error bars: 95% confidence interval of adjusted values based on analysis of variance (ANOVA).

### 3.2. Single doping

Figs. 8 and 9 give the RIT and the grain size results, respectively, for pure and single 450 ppm-doped alumina samples as a function of the sintering pressure and soak temperature. From these figures, we observe that the introduction of dopants (MgO, Y<sub>2</sub>O<sub>3</sub> and La<sub>2</sub>O<sub>3</sub>) increases the RIT and reduces the grain size under all investigated sintering conditions.

For pure alumina, the SEM image in Fig. 6(a) shows that inter- and intragranular pores as well as grain growth are responsible for the poor RIT values. This can be explained by both insufficient densification and pore grain boundary separation during rapid grain growth in the final stage of sintering, which occurs due to the absence of an effective grain boundary movement inhibitor.

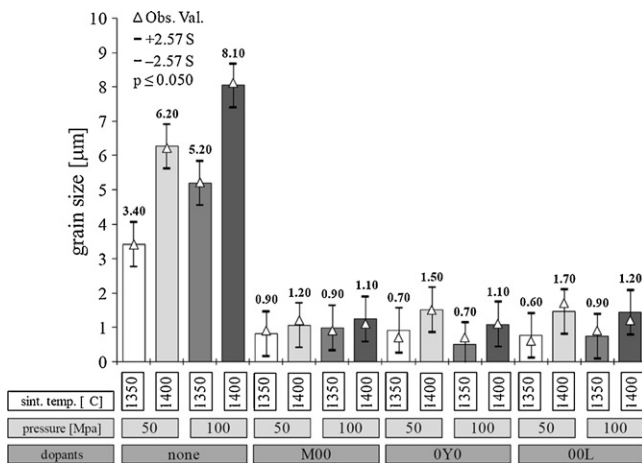


Fig. 9. Grain size diameter (bold numbers = measured values) as a function of dopant elements (450 ppm), sintering pressure and final sintering temperature. Heating rate:  $\sim 100^\circ\text{C}/\text{min}$ . Error bars: 95% confidence interval of adjusted values based on analysis of variance (ANOVA).

For all doping strategies an increase of the sintering temperature from  $1350^\circ\text{C}$  to  $1400^\circ\text{C}$  at both 50 MPa and 100 MPa leads to larger grains. The RIT however is observed to either improve or deteriorate depending on the pressure. At 50 MPa, an increase of the sintering temperature enhanced the RIT values whereas at 100 MPa the RIT decreased. We can assume that densification is enhanced by the application of pressure, therefore higher pressures are expected to reduce the sintering temperature required for full densification. The improvement in the RIT at 50 MPa on increasing the temperature is due to an enhanced densification, whereas at 100 MPa densification is complete earlier and increased grain growth reduces the RIT at  $1400^\circ\text{C}$ . Therefore, it can be concluded that in this case a sintering pressure of 100 MPa is sufficient to guarantee full densification at  $1350^\circ\text{C}$  (c.f. sensitivity of RIT on porosity and grain size, Fig. 1).

Comparing the single doping strategies between each other in terms of RIT and grain sizes, it seems that Mg doping reduces the sensitivity to the sintering parameters, in particular on the temperature change at high pressure. As can be seen from Figs. 8 and 9, at 100 MPa the RIT of 450 ppm Mg-doped PCA drops slightly from 40.1% (grain size  $0.88\ \mu\text{m}$ ) to 35.2% ( $1.09\ \mu\text{m}$ ) upon increasing the sintering temperature from  $1350^\circ\text{C}$  to  $1400^\circ\text{C}$ . Whereas for 450 ppm Y- and La-doped PCA the RITs fall more severely from 54.8% ( $0.73\ \mu\text{m}$ ) to 40.5% ( $1.11\ \mu\text{m}$ ) and 48.8% ( $0.89\ \mu\text{m}$ ) to 32.6% ( $1.22\ \mu\text{m}$ ), respectively. Y and La therefore seem to have a similar effect, which however strongly depends on the sintering parameters, although Y seems slightly more effective than La in reducing grain growth. The reduced sensitivity of the RIT (grain size) on the sintering parameters of Mg-doped alumina may be explained by enhanced grain boundary diffusion and the surface roughening effect.<sup>14,18,20</sup>

From Fig. 9 it is interesting to note that at any sintering temperature and whatever dopant element, an increase of the sintering pressure generally reduces grain growth. For pure alu-

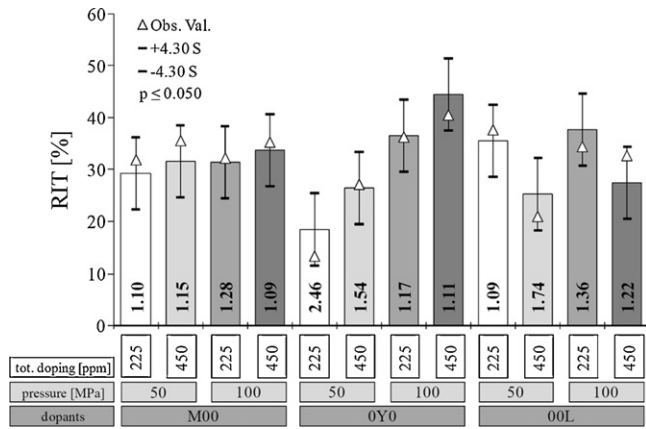


Fig. 10. Real inline transmittance as a function of dopant elements, sintering pressure and total doping level. Bold numbers are the measured grain size diameter values by line intercept method. Sintering temperature: 1400 °C; heating rate: 100 °C/min. Error bars: 95% confidence interval of adjusted values based on analysis of variance (ANOVA).

mina, increased sintering pressure (from 50 MPa to 100 MPa) leads to significant grain growth, whereas for the Mg-doped samples the pressure has almost no effect. For Y and La doping, the grain size is clearly reduced from 1.50 μm to 1.10 μm and 1.70 μm to 1.20 μm, respectively, at 1400 °C when pressure is increased from 50 MPa to 100 MPa. Taking into consideration the fact that higher applied pressures lead to an enhanced grain growth above a critical temperature,<sup>30</sup> the addition of dopants seems to increase this temperature. The enhanced grain growth for pure alumina under increased pressure has also been reported for HIP sintered samples<sup>31</sup> and is known to be dependent on the sintering temperature, the density of the ceramic to be sintered. The critical values of these parameters can be influenced by the doping strategies<sup>31,32</sup> as we have also observed here.

Fig. 10 gives the RIT for single-doped alumina samples sintered at 1400 °C as a function of the doping level and the sintering pressure. It appears that for Mg and Y doping an increase of the doping level leads to an increase of the RIT from 31.8% to 35.5% and 13.4% to 27.1%, respectively, at 50 MPa. The increase of the doping level is less important at high sintering pressure (32.1–35.2% for Mg doping and 36.2–40.5% for Y doping at 100 MPa). For La doping an increase of the doping level from 225 ppm to 450 ppm leads to a reduction in RIT which is accompanied by increased grain size. For example the decrease in RIT from 37.6% to 20.9% is explained by an increased grain size passing from 1.09 μm to 1.74 μm at 1400 °C and 50 MPa, the effect being less marked under higher pressure. The reasons for this are currently being investigated. It can be seen again that Mg doping reduces the sensitivity of RIT to both sintering pressure and doping level in the ranges studied.

### 3.3. Double and triple doping

To avoid too much interference from porosity on the analysis of the effects of double and triple doping on the RIT, only the samples sintered at 1400 °C have been used for the comparative study.

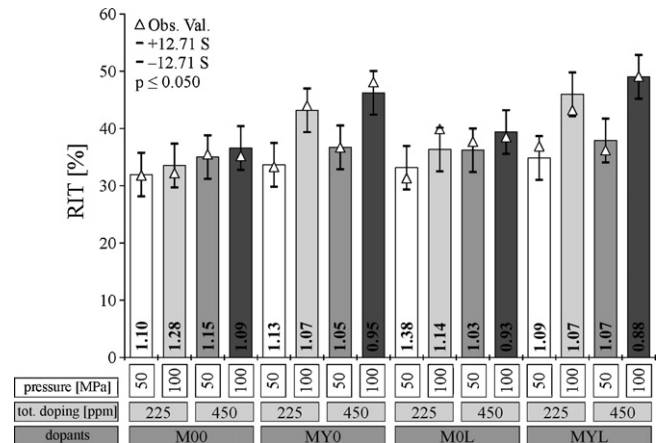


Fig. 11. Real inline transmittance as a function of dopant elements, total doping level and sintering pressure. Bold numbers are the measured grain size diameter values by line intercept method. Sintering temperature: 1400 °C. Heating rate: 100 °C/min. Error bars: 95% confidence interval of adjusted values based on analysis of variance (ANOVA).

Firstly, the double doping effect is investigated by comparing the samples containing the same absolute single dopant level. Comparing 225:M00 with 450:MY0 and 450:M0L in Fig. 11 (i.e. 225 ppm Mg in each), it can be observed that the addition of Y or La improves the RIT regardless of the sintering pressure. This is supported by a slightly reduced grain size. Similarly, by comparison of 225:OY0 and 225:O0L with 450:OYL (Fig. 12), 225:O0L with 450:M0L (Figs. 11 and 12) and 225:OY0 with 450:MY0 (Figs. 11 and 12), it can be observed that double doping always leads to some improvement in RIT with reduced or slightly reduced grain size.

Comparing the three different double doping strategies (MY0, M0L, and OYL) with the three single doping strategies at both 225 ppm and 450 ppm, respectively, it appears that the double doping strategies improve the RIT, except for 225:OYL sintered at 1400 °C/50 MPa which is not fully dense. Further

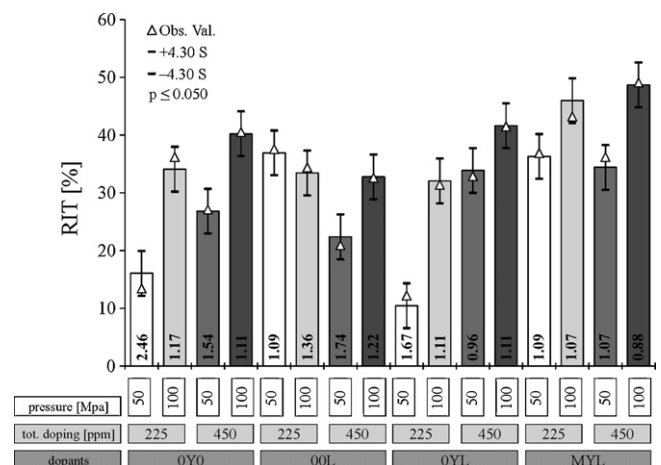


Fig. 12. Real inline transmittance as a function of dopant elements, total doping level and sintering pressure. Bold numbers are the measured grain size diameter values by line intercept method. Sintering temperature: 1400 °C. Heating rate: 100 °C/min. Error bars: 95% confidence interval of adjusted values based on analysis of variance (ANOVA).

Table 1  
Best RIT results for each doping strategy (@ 100 MPa).

Dopants	225 ppm		450 ppm	
	RIT [%]	Soak temp. [°C]	RIT [%]	Soak temp. [°C]
M00	32.17	1400	52.27	1250 <sup>a</sup>
OY0	55.19	1310 <sup>a</sup>	54.71	1350
O0L	52.56	1350 <sup>a</sup>	50.10	1370 <sup>a</sup>
MY0	48.34	1350	54.76	1350
M0L	51.31	1330 <sup>a</sup>	54.63	1350
OYL	56.89	1350	49.37	1350
MYL	55.77	1330 <sup>a</sup>	56.95	1350

RIT for 0.8 mm @ 640 nm.

<sup>a</sup> Samples from “optimized” series.

it can be noted that Mg addition to Y or La increases the RIT and reduces the sensitivity on the doping level and pressure. Finally, the negative effect observed for single La doping, where an increase of the doping level leads to a decrease of the RIT, can be reversed by adding Mg or La. However it is not possible to attribute this effect totally to Mg or Y addition as the absolute La amount is reduced by a factor of 2 for the double doping strategy as the total doping concentration remains constant.

Considering the triple doping effect, regardless of using the single species or total dopant cationic ratio, triple (MYL) doping gives better RIT values than any double doping strategy at 1400 °C (Figs. 11 and 12). This indicates that the synergetic effect has been enhanced further in the triple doping strategy compared with the double doping strategies.

Considering the general positive effects generated by Mg addition for the double, M0L and MY0, as well as triple doping strategies, the following mechanism can be proposed. Since Mg is commonly admitted to create oxygen vacancies due to the local electroneutrality condition, it might be argued that Mg addition increases the amount of favorable Y or La accommodation sites (vacancy and atomic size combination effects), this is currently under investigation by atomistic modeling based on the single dopant study using the energy minimization approach.<sup>25</sup> In fact, Mg is often reported to cause grain surface roughening, which might explain its liquid scavenger properties by increasing the amount of favorable atom accommodation sites.<sup>14,18–20</sup>

### 3.4. Sintering parameters optimization

In order to get minimum grain growth but still ensure full densification, both sintering temperature and pressure have to be optimized as shown in the previous sections. To illustrate the effect of this optimization, a series of doped samples were sintered at 100 MPa with the sintering temperature adjusted to 50 °C above the densification peak observed on the densification curve for samples sintered at 1400 °C and 50 MPa. The overall best RIT results obtained for each doping strategy are summarized in Table 1. By using the temperature and pressure best adapted for each dopant combination, all the doped alumina ceramics (regardless of single, double or triple doping of Mg, Y and La) can be sintered with a RIT close to or above 50% with good reliability by using SPS. The best result is 50%

better than any other published results for SPS. Meanwhile, it should be emphasized again that the similarities in terms of RIT regardless of the doping strategies achieved from the optimized conditions do not necessarily disagree with the doping effects discussed in the previous sections. In fact the sintering temperature and pressure play the predominant role under optimized sintering conditions, reducing the apparent effect of the dopants. The present simple optimization does not exclude further optimization which may show the intrinsic dopant effects and lead to further improvement in RITs.

To compare the effectiveness of the dopant nature, the triple-doped (450:MYL) and three double-doped (225:MY0, 225:M0L and 225:OYL) results are compared in detail as they have similar doping levels (112.5 ppm for double doping and 150 ppm for triple doping) for each dopant cation (Mg, Y, La). 450:MYL gives a better RIT than 225:MY0 and 225:M0L but not significantly better than 225:OYL. This indicates that Y and La are more efficient grain growth inhibitors than Mg in this range of sintering temperatures and pressures. Detailed explanations of such synergistic doping effects cannot be given at this time, but are being investigated both experimentally and theoretically by atomistic simulation methods. It might be possible that spaces in the grain boundary area can be filled more efficiently by combining Y and La (e.g. different cation sizes), increasing the energy barrier (i.e. stress) to be overcome for atoms to move across the grain boundary and contribute to grain growth.

To show the effect of dopants on the optical appearance of the samples, two optimized samples pure Al<sub>2</sub>O<sub>3</sub> and 450:MYL are shown in Fig. 13.

Finally a series of experiments were carried out varying the heating rate, the moment of pressure application, the pulse sequence and an intermediate holding stage during the heating.

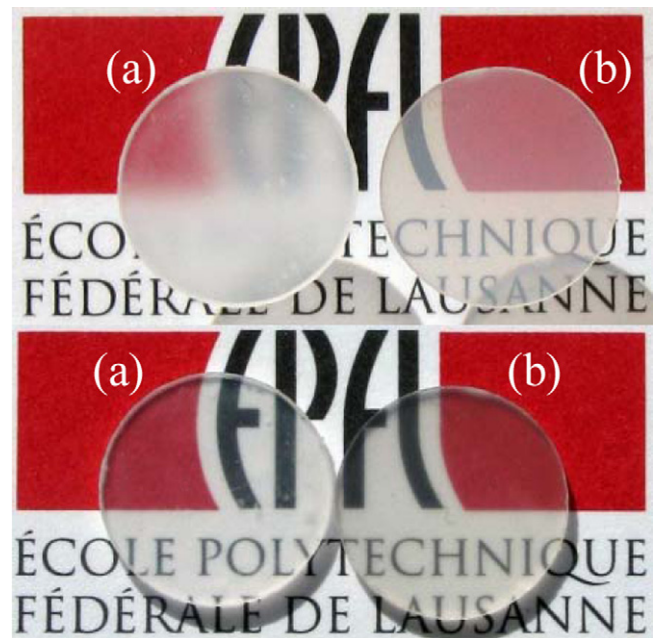


Fig. 13. (a) Undoped PCA sample ( $\varnothing$  12 mm) with RIT of 7.8%; (b) 450:MYL PCA sample with RIT of 57%; top: 1.5 cm above the sheet (through Plexiglas); bottom: placed directly on the sheet.

Table 2  
RIT results for different sintering parameters for 450 ppm Mg-doped alumina samples sintered at 1300 °C and 100 MPa.

Sintering parameter	Value	RIT [%]
Heating rate [°C/min]	100	53.6
	233	50.8
	350	48.9
Holding temperature for 3 min [°C]	No	53.6
	900	53.5
	1000	53.9
	1100	52.7
Moment of pressure application	Whole cycle	53.6
	At sint. temp.	53.7
Pulse sequence [on:off]	12:2	53.6
	10:9	53.5
	3:2	53.5

Grey background: studied parameter has no influence.

Except for the heating rate, the increase of which reduces the RIT, none of the other SPS sintering parameters had a significant influence on the RIT (Table 2). However the variation of such parameters might be of interest to solve other problems in future. In fact crystalline defect creation due to high sintering pressures combined with low sintering temperature (e.g. plastic deformation, dislocation climbing) seems to influence the coloration of the samples and needs to be further investigated. Note that the results for the parameters in Table 2 that have no significant influence, demonstrate the high reproducibility attainable with SPS for the production of transparent PCA.

#### 4. Conclusions

Spark plasma sintering (SPS) of doped (Mg, Y, La) submicron  $\alpha$ -alumina has been investigated. It has been shown that SPS is a reliable and reproducible method for the production of transparent polycrystalline alumina (PCA) pieces with real inline transmittances (RITs) >50% ( $\lambda = 640$  nm, 0.8 mm thickness). Despite the short sintering cycles of SPS (typically 15 min), it was found that doping is required to achieve good optical properties of PCA. SPS of pure alumina cannot avoid extensive grain growth and results in pore grain boundary separation, which is effectively, suppressed by the use of Mg, Y and La dopants. The use of co-doping of each of the different pairs generally improves the RIT by reducing the grain size compared with single doping strategies.

Triple Mg, Y and La doping in equal proportions with a total cationic ratio of 450 ppm gave the best real inline transmittance (RIT) performance with 57%, 50% higher than previously published SPS studies. Such high RITs can only be achieved by SPS, if high sintering pressures and low sintering temperatures are used. Furthermore high heating rates have a negative effect. The results in this study should open the way for further investigation and improvement of transparent polycrystalline alumina produced using rapid sintering techniques such as SPS.

#### Acknowledgments

European Union is acknowledged for the partly funding of the current work through the IP-NANOKER project (NMP3-CT-2005-515784). Solvadis Chemag GmbH (Frankfurt am Main, Germany) and Céramaret SA (Bôle, Switzerland) are acknowledged for the powder supply and the sample polishing, respectively. Dr. Xin Wang is acknowledged for SEM imaging. We also would like to appreciate the EM facility support from Knut and Alice Wallenberg Foundation.

#### References

1. Apetz R, van Bruggen MPB. Transparent alumina: a light-scattering model. *J Am Ceram Soc* 2003;**86**:480–6.
2. Jiang D, Hulbert DM, Anselmi-Tamburini U, Ng T, Land D, Mukherjee AK. Optically transparent polycrystalline  $\text{Al}_2\text{O}_3$  produced by spark plasma sintering. *J Am Ceram Soc* 2008;**91**:151–4.
3. Krell A, Blank P, Ma HW, Hutzler T, van Bruggen MPB, Apetz R. Transparent sintered corundum with high hardness and strength. *J Am Ceram Soc* 2003;**86**:12–8.
4. Krell A, Klimke J. Effects of the homogeneity of particle coordination on solid-state sintering of transparent alumina. *J Am Ceram Soc* 2006;**89**:1985–92.
5. Krell A, Klimke J, Hutzler T. Advanced spinel and sub- $\mu\text{m}$   $\text{Al}_2\text{O}_3$  for transparent armour applications. *J Eur Ceram Soc* 2008.
6. Wei GC. Transparent ceramic lamp envelope materials. *J Phys D: Appl Phys* 2005;**38**:3057–65.
7. Peelen JGJ, Metselaar R. Light-scattering by pores in polycrystalline materials: transmission properties of alumina. *J Appl Phys* 1974;**45**:216–20.
8. Krell A, Hutzler T, Klimke J. Transmission physics and consequences for materials selection, manufacturing, and applications. *J Eur Ceram Soc* 2009;**29**:207–21.
9. Bernard-Granger G, Guizard C. Influence of MgO or  $\text{TiO}_2$  doping on the sintering path and on the optical properties of a submicronic alumina material. *Scr Mater* 2007;**56**:983–6.
10. Bernard-Granger G, Guizard C, Addad A. Influence of co-doping on the sintering path and on the optical properties of a submicronic alumina material. *J Am Ceram Soc* 2008;**91**:1703–6.
11. Krell A, Blank P, Ma HW, Hutzler T, Nebelung M. Processing of high-density submicrometer  $\text{Al}_2\text{O}_3$  for new applications. *J Am Ceram Soc* 2003;**86**:546–53.
12. Shiau FS, Fang TT, Leu TH. Effects of milling and particle size distribution on the sintering behavior and the evolution of the microstructure in sintering powder compacts. *Mater Chem Phys* 1998;**57**:33–40.
13. Zheng JM, Reed JS. Effects of particle packing characteristics on solid-state sintering. *J Am Ceram Soc* 1989;**72**:810–7.
14. Berry KA, Harmer MP. Effect of MgO solute on microstructure development in  $\text{Al}_2\text{O}_3$ . *J Am Ceram Soc* 1986;**69**:143–9.
15. Fang JX, Thompson AM, Harmer MP, Chan HM. Effect of yttrium and lanthanum on the final-stage sintering behavior of ultrahigh-purity alumina. *J Am Ceram Soc* 1997;**80**:2005–12.
16. Kim BN, Hiraga K, Morita K, Yoshida H, Miyazaki T, Kagawa Y. Microstructure and optical properties of transparent alumina. *Acta Mater* 2009;**57**:1319–26.
17. Shen, Z., Zhao, Z., Johnsson, M., and Nygren, M., Swedish Patent SE0303403A, 2005.
18. Bennison SJ, Harmer MP. Grain-growth kinetics for alumina in the absence of a liquid-phase. *J Am Ceram Soc* 1985;**68**:C22–4.
19. Jo W, Kim DY, Hwang NM. Reply to the comment on “Effect of interface structure on the microstructural evolution of ceramics”. *J Am Ceram Soc* 2007;**90**:2293–5.
20. Park CW, Yoon DY. Effects of  $\text{SiO}_2$ ,  $\text{CaO}_2$ , and MgO additions on the grain growth of alumina. *J Am Ceram Soc* 2000;**83**:2605–9.

21. Jo W, Kim DY, Hwang NM. Effect of interface structure on the microstructural evolution of ceramics. *J Am Ceram Soc* 2006;**89**:2369–80.
22. Sato E, Carry C. Yttria doping and sintering of submicrometer-grained  $\alpha$ -alumina. *J Am Ceram Soc* 1996;**79**:2156–60.
23. Voytovych R, MacLaren I, Gulgun MA, Cannon RM, Ruhle M. The effect of yttrium on densification and grain growth in alpha-alumina. *Acta Mater* 2002;**50**:3453–63.
24. Bouchet D, Lartigue-Korinek S, Molins R, Thibault J. Yttrium segregation and intergranular defects in alumina. *Philos Mag* 2006;**86**:1401–13.
25. Galmarini S, Aschauer U, Bowen P, Parker SC. Atomistic simulation of Y-doped  $\alpha$ -alumina interfaces. *J Am Ceram Soc* 2008;**91**:3643–51.
26. Cho JY, Rickman JM, Chan HM, Harmer MP. Modeling of grain-boundary segregation behavior in aluminum oxide. *J Am Ceram Soc* 2000;**83**:344–52.
27. Bae SI, Baik S. Critical concentration of MgO for the prevention of abnormal grain-growth in alumina. *J Am Ceram Soc* 1994;**77**:2499–504.
28. Montgomery DC. *Design and Analysis of Experiments*. 3rd ed. New York: Wiley; 1991.
29. Mendelson MI. Average grain size in polycrystalline ceramics. *J Am Ceram Soc* 1969;**52**:443–6.
30. Shen ZJ, Johnsson M, Zhao Z, Nygren M. Spark plasma sintering of alumina. *J Am Ceram Soc* 2002;**85**:1921–7.
31. Besson J, Abouaf M. Grain-growth enhancement in alumina during hot isostatic pressing. *Acta Metall Mater* 1991;**39**:2225–34.
32. Park H, Park SY. Grain growth behavior of alumina during sinter-HIP process. *J Mater Sci Lett* 2001;**20**:601–3.